A comprehensive study on Ni-Doped cobalt ferrites for optical response and anti-bacterial activity

F. Ullah[a], I. Ahmad[b], S. Zaib[c], M. Abrar[c], M. Khalil[d], M. A. Ebdah[e], S. M. Ramay[e], M. Saleem[f,*]

[a]*Department of Physics, University of Azad Jammu and Kashmir, Muzaffarabad, 13100, Pakistan*

[b]*Department of Physics, Government Degree College Balakot, Mansehra, Khyber Pakhtunkhwa, Pakistan*

[c]*Department of Physics, Hazara University, Mansehra, Khyber Pakhtunkhwa, Pakistan*

[d]*Department of Physics, University of the Punjab, Quaid-e-Azam Campus, Lahore 54000, Pakistan*

[e]*Physics and Astronomy Department, College of Science, King Saud University, Riyadh 11451, Saudi Arabia*

[f]*Department of Physics, Syed Babar Ali School of Science and Engineering, Lahore University of Management Sciences (LUMS), Lahore-54792, Pakistan*

In the current study, Ni doped $CoFe_2O_4$ nanoparticles were fabricated using well-known hydrothermal method. The structural, morphological, optical, and antibacterial activity were analyzed through the latest analytical techniques. The F*d*-cubic spinel crystal structure was observed with variations in crystallite sizes and lattice parameters of synthesized samples. The growth of spherical and uniform nanoparticles with the presence of expected elements are observed from field emission scanning electron microscopy and energy dispersive x-rays analysis, respectively. A broad absorption band was shown in UV-visible absorption spectroscopy in the wavelength range of 200-320 nm. A significant increase in the energy band gap was observed from 2.98 eV to 3.56 eV as the concentration of dopant increased from 2% to 6%. The antibacterial activities of the samples were investigated against *Staph aureus*, *Pseudomonas aeruginosa* and *E. Coli* through the well-known Agar well diffusion method. The pure and Ni-doped $CoFe_2O_4$ exhibits a maximum zone of inhibition (3-25 mm), proposing that these materials are efficient against bacterial resistance. Further, the enhancement in value of the inhibition zone by substitution of Ni at cobalt sites recommended that it is a potential candidate for biomedical applications and can be highly effective against the high resistance of different bacteria.

(Received May 23, 2023; Accepted August 9, 2023)

Keywords: Cobalt-ferrite, Nanoparticles, Optical properties, Antibacterial, Gram positive bacteria and gram-negative bacteria

1. Introduction

Ferrites are a type of ceramics with black or gray in color, containing iron oxide and metals, generally having formula $A(Fe_2O_4)$ here *A* shows divalent ions of different metals (Co^{2+}, Zn^{2+}, Ni^{2+}, $Mn^{2+,}$ etc). The ion distribution is in such a way that its metal cations are on tetrahedral sites while oxygen ions are octahedrally distributed. It can be classified into four categories on the bases of its structure: garnets, spinel, ortho, and hexagonal ferrites [1]. In the last few years, researchers have focused on spinel metal ferrite (e.g., M = Mn, Cu, Zn, Ni, etc) which attain

* Corresponding author: murtaza.saleem@lums.edu.pk
https://doi.org/10.15251/DJNB.2023.183.975

interesting physical properties and have attractive applications-based properties such as target drug delivery, antibacterial performance against resistant bacteria and catalysis activities [2-9].

The most outstanding properties of ferrites are their antibacterial performance which can be enhanced by doping and coating with organic, inorganic, metal, or nonmetal materials. The spinel ferrite prepared simply and nontoxic can be widely used in different applications. The antibacterial effect of spinel ferrite can also be enhanced by modifications of surface morphology, particle size, phase components, and microstructure. Among these spinel ferrites, cobalt ferrite ($CoFe_2O_4$) has good attractive properties such as increased drug solubility, decrease side effects, and high stability and due to these properties, it has very extensive attention in pharmaceutical medicinal applications [10,11]. Furthermore, metal ferrite ($NiFe_2O_4$, $CoFe_2O_4$, etc) nanoparticles have been widely used in different biomedical applications such as cancer treatment by MRI and hyperthermia [12-14]. Kinza et al. [15] recorded an antibacterial effect maximum zone of inhibition in the range of 10-16 mm for pure and Ag metal doped $CoFe_2O_4$ against EDR (Extensively Drug resistance) pathogens *P. aeruginosa* and *E. coli*, and MDR (Multi-Drug-Resistance) pathogen *S. aureus* also suggested that these materials are a good candidate for biomedical applications.

Various researchers have used different physical and chemical methods such as; coprecipitation, sol-gel, reverse micelle, combustion, hydrothermal, microwave, and electrochemical method for the synthesis of $MCoFe_2O_4$ [16-18]. Among these methods, the hydrothermal route received much attention due to offering a lot of advantages such as control over composition and morphologies, phase and size transformation, diffusion, enhancement of solubility, environmentally friendly, the prepared sample does not require post-treatment processes like calcination but the most attractive is its lower synthesis temperature such as 150 °C the crystalline nanoparticle of ferrite can be prepared [19-23]. In the current study, we investigated the antibacterial and optical response of Ni doped $CoFe_2O_4$ composition prepared via hydrothermal route. Further, the structural, morphological, optical, and antibacterial properties of these compositions with different characterization techniques were briefly studied for investigation of optical and biomedical applications.

2. Materials and methods

2.1. Samples preparations

The well-known hydrothermal approach was used for synthesizes of pure and Nickle doped $CoFe_2O_4$ nanostructured with varying concentrations ($Ni_xCo_{1-x}Fe_2O_4$ where x = 0%, 2%, 4% and 6%) [24]. The calculated-stoichiometric amount of different chemicals i.e., Ferric nitrate [Fe $(No_3)_3.9H_2O$], Cobalt nitrate [Co $(No_3)_2$], and Ni nitrate [Ni $(NO_3)_2.6H_2O$] were used as the raw materials sources of Fe, Co, and Ni, respectively. The chemicals have a purity of 99.95% purchased from BDR-AnalaR and were used without any further modifications and purification. Initially, Fe-nitrate and Co-nitrate were dissolved in 40ml of deionized (D.I) water in a beaker and stirred at low temperature for 1h. The sodium hydroxide (NaOH) dissolved in water was used as a reducing agent, and to get a homogenous solution; NaOH was added dropwise to the mixed solution till the pH of the solution was adjusted up to 12. In order, to complete the reaction: this homogenous solution was shifted to Teflon-lined-autoclave and heated for 16h at 160 ºC. Further, after completion of the reaction, the autoclave was cooled down to RT (room temperature), and synthesized particles were centrifuged, filtered, and washed with ethanol and D.I water to several times for the removal of extra impurities completely. Finally, to get the product in completely powder form, compositions were dried overnight at 80 ºC in an oven.

2.2. Antibacterial activity

For the antibacterial activity of $Ni_XCo_{1-x}Fe_2O_4$ where x = 0, 0.98/2%, 0.96/4%, and 0.94/6% were tested by using the well-known Agar-well diffusion method [24]. Initially, the volume of pure culture of three different bacterial strains i.e., *Staph-aureous, E.Coli,* and *Psedomenas aeroginosa* was spread on whole agar-plates and then with help of Cork borer a 5 mm hole was made. The holes were loaded with different concentrations of nanoparticles and DMSO

solution. Then for further processing, these plates were placed in an incubator for 24 h at 37 ºC. Finally, the zone of inhibition measurements was done after the collection of plates from an incubator.

2.3. Instrumentations

The structural parameters such as, lattice constant, crystallite size, and cell volume of pure and Ni-doped $CoFe_2O_4$ were studied through X'pert Pro-multipurpose diffractometer *MPD*. The voltage and current of the diffractometer were kept up to 40 kV and 40 mA, respectively along with the Cu-K_α radiations (wavelength 0.154 nm) were used. The morphological studies were done by using Field Emission Scanning Electron Microscopy *FESEM* of model FEI Nova (Nano SEM-450). The micrographs of these compositions were observed at different magnifications range and the electron beam energy was 10 kV. The TLD lens detector was used in their secondary mode and the working distance was adjusted to approximately 5.0 mm. The qualitative and quantitative analysis i.e., elemental composition analysis were performed via Energy Dispersive X-ray Spectroscopy *EDS* model Inca x-Act Oxford. The band gap and absorption spectra were extracted UV-vis (ultraviolet-visible) spectrophotometer Shimadzu, UV-1800. Finally, agar well disc diffusion methods were used for antibacterial activities.

3. Results and discussion

3.1. Crystallographic studies

An X-ray diffractometer was used for the crystallographic study of synthesized pure and Ni-doped $CoFe_2O_4$ nanoparticles. Figure 1 shows the XRD peaks pattern of these samples. The different diffraction peaks at 2θ positions of 30.67º, 36.00º, 43.67º, 57.55º and 63.25º attributes to the plane (220), (311), (400), (511), and (440), respectively. The indexed peaks of pure and Ni-doped $CoFe_2O_4$ compositions confirm cubic spinel structure and these peaks matched with JCPDS reference card # 22-1086 exhibit space group, F*d*-3m. In XRD patterns, no extra peak was observed which highlighted the phase purity of all compositions. The highest peaks in these patterns are shown at 36.0º which corresponds to (311) planes having the most intense reflection and confirms the highest crystallinity of these samples as shown in the literature [25]. For these compositions, the exact matching of all indexed peaks at angle 2θ shows the stability of structure with substituted at Co-sites as well as agrees with the previous literature that dopant concentration less than 15% does not disturb its stability [26].

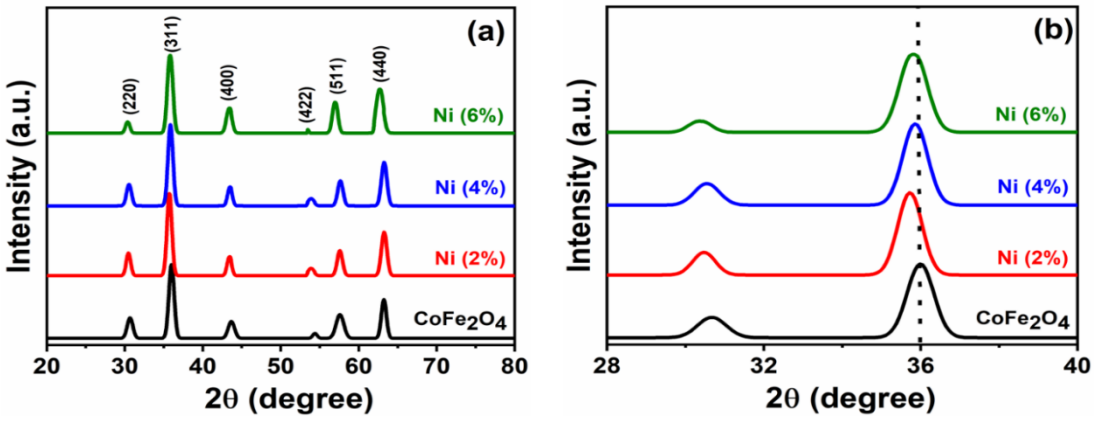

Fig. 1. XRD spectra results (a) Full peaks pattern and (b) Highest crystallite peaks of pure and Ni (2%, 4%, and 6%) $CoFe_2O_4$.

Table 1. Crystallographic study parameters computed from XRD analysis of undoped and Ni doped $CoFe_2O_4$ compositions.

Parameters	$CoFe_2O_4$	2%-Ni	4%-Ni	6%-Ni
2θ (°)	36.10	35.87	35.73	35.68
$d_{spacing}$*(Å)*	2.494	2.514	2.529	2.540
FWHM (rad)	0.799	0.734	0.691	0.672
Crystallite-size(nm)	10.83	12.21	14.90	17.96
Lattice constant	8.266	8.306	8.325	8.350
Cell volume(a^3)	564.73	572.97	577.02	582.27
Lattice strain	0.526	0.450	0.430	0.405

The crystallite size of all samples was calculated by using the well-known Scherrer's relation [27]:

$$D = \frac{K\lambda}{\beta cos\theta} \quad (1)$$

where *D* and *K* represent crystallite size proportionality and 0.9, λ X-rays wavelength and proportionality. The crystallite size values were calculated as 10.83 nm, 12.21 nm, 14.90 nm, and 17.96 nm for pure, 2 wt.%, 4 wt.%, and 6 wt.% Ni doped $CoFe_2O_4$ spherical nanoparticles, respectively and the enhancement in crystallite size is expected due to the difference in ionic radii of dopant Ni^{2+} (0.72 Å) and host Co^{2+} ions (0.76 Å) as reported in Kinza et al. work [15]. Furthermore, the lattice constant *a*, cell volume *V*, microwave strain *ε*, and dislocation density *δ* for pure and Ni-doped $CoFe_2O_4$ were calculated by the given equations below equations [27]:

$$a = dhkl\ (h^2 + k^2 + l^2)^{1/2} \quad (2)$$

$$V = a^3 \quad (3)$$

$$\varepsilon = \beta/4\tan\theta \quad (4)$$

$$\delta = 1/D^2 \quad (5)$$

In these equations a represents lattice constant, d spacing between two planes and hkl represents miller indices. The lattice constant values vary from 8.226 Å-8.356Å while strain and dislocation density decrease as Ni^{2+} ions concentrations is enhanced due to improvement in crystallinity by a decrease in misfit in the lattice of unit cells.

3.2. Morphological studies

The morphological study of pure and Ni-doped $CoFe_2O_4$ was performed via the FESEM technique as presented in Figure 2. In this context, the grains' size, shape, porosity, and growth of grains along boundaries were analyzed. The high and low-magnification micrographs were shown in Figure 2(a-d). It can be seen from all the micrographs that grains are spherical with well-defined grain boundaries. The size of spherical grains is in the range of 20-33 nm. The spherical particles of pure and Ni-doped $CoFe_2O_4$ compositions have uniform size and regular shape, but there are also large-size grains present due to the sintering of a few small-size grains.

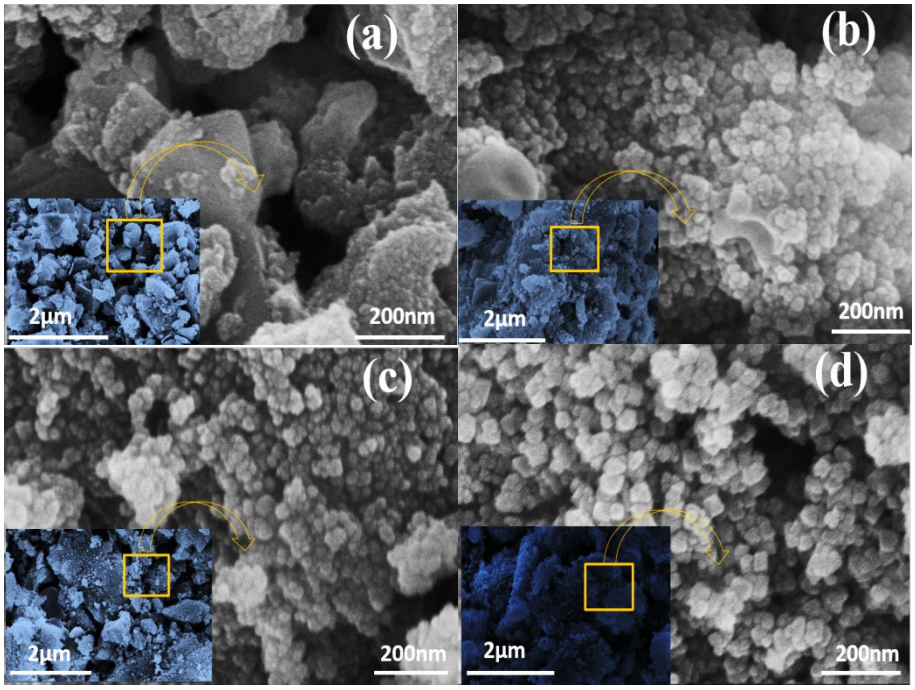

Fig. 2. FESEM micrographs at low(2µm) and high(200nm) magnifications; here (a) Pure $CoFe_2O_4$, (b) 2 wt.% Ni doped, (c) and (d) 4 & 6 wt.% Ni doped $CoFe_2O_4$ spherical nanoparticles compositions.

The diameter of spherical shape particles was calculated from FESEM images using Image-J software presented using particle distribution histogram [28], as shown in Figure 3. The average particle size is recorded as 20.18, 25.03, 30.01, and 33.95 nm for pure, 2wt.%, 4wt.%, and 6wt.% Ni doped $CoFe_2O_4$ respectively. This shows that as the Ni concentration increases the size of particles is enhanced. The effect is also shown in the case of crystallite size due to varying ionic radii of Ni as compared to host material Cobalt as discussed in the XRD section.

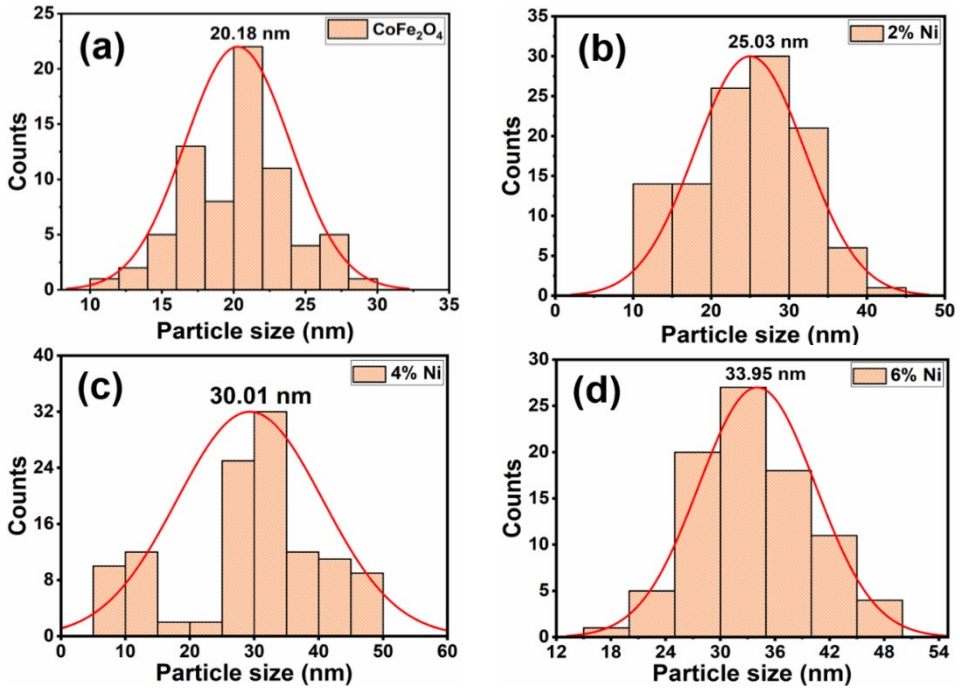

Fig. 3. Histogram plot extracted from FESEM micrographs through Image-J technique of (a) Pure $CoFe_2O_4$, (b) 2 wt.% Ni doped, (c) and (d) 4 & 6 wt.% Ni doped $CoFe_2O_4$ nanoparticles.

3.3. Energy Dispersive X-rays (EDX) analysis

Energy dispersive x-ray spectroscopy was used for the quantitative and qualitative analysis of pure and Ni-doped $CoFe_2O_4$ compositions. Figure 4 shows the EDX spectrum and confirms the high concentration peaks of Fe, Co, and O for pure and Ni also in 2wt.%, 4wt.%, and 6wt.% approximately. The intense peaks shown in figure 4(a-d) lie at the same value on the energy axis and show the presence of elements with their empirical formulation and pure growth of pure and Ni-doped $CoFe_2O_4$ samples. The quantitative details of all samples given in table 2 confirm the presence of required elements in each composition with their exact stoichiometric ratio. In spectrums, the gold *Au* peaks were appear because to reduce the conduction of ferrite with the focused electron beam, the samples were coated with gold sputtered.

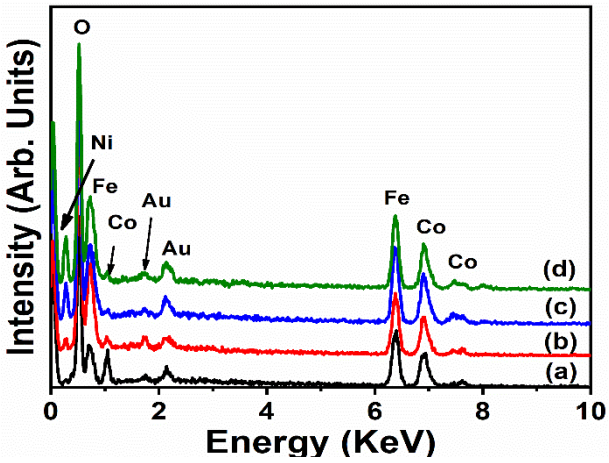

Fig. 4. Energy dispersive x-rays spectra of (a) Pure $CoFe_2O_4$, (b) 2 wt.% Ni doped, (c) 4 wt.% Ni doped and (d) 6 wt.% Ni doped $CoFe_2O_4$ compositions.

Table 2. Elemental compositions observed through EDX analysis by wt.% of hydrothermally synthesized pure and Ni-doped samples.

	$CoFe_2O_4$	*2%-Ni doped*	*4%-Ni doped*	*6%-Ni doped*
Elements	Wt.%	Wt.%	Wt.%	Wt.%
O(k)	45.55	47.38	45.81	46.43
Fe(k)	34.18	32.1	33.72	31.97
Co(k)	18.25	17.86	17.15	17.63
Ni(k)	—	0.37	0.8	1.15
Au(M)	2.02	2.29	2.52	2.82
	100	100	100	100

3.3. Optical properties

Figure 5 shows the optical response of pure and Ni-doped Cobalt ferrite nanoparticles studies through UV-visible spectroscopy technique in the UV-visible range of 200 -700 nm. Figure 5(a) shows absorption spectra of pure CoF_2O_4 have a broad range from ~260 to ~340 nm having peak positions ~305 nm while the absorption spectrums range from ~215 to 350 nm having maxima peaks position ~280 nm, ~285 nm and ~290 nm observed for 2wt.%, 4wt.% and 6wt.% Ni-doped $CoFe_2O_4$ respectively shifted towards lower wavelength which strongly affects energy band gap, calculated by Tauc relation:

$$(\alpha.h\upsilon)^{n} = K\,(h\upsilon - E_g) \qquad (6)$$

where α represents the absorption coefficient, K and E_g are constant of material and optical band gap value respectively, $h\nu$ is photon energy and n = ½ for an indirect while for direct transition n = 2. The energy band gap values are observed in the range 2.99, 3.47, 3.56, and 3.36 eV for pure, 2%, 4%, and 6% Ni-doped $CoFe_2O_4$ compositions respectively. The increment occurs by substitution of Ni-content at Co-sites credited to the fact that ionic radii of Ni-ions (0.072 nm) are smaller than Co-ions (0.074 nm) and these results from stronger electrostatic interaction. This stronger interaction forms deeper Ni-sites than Co-sites hence increasing the band gap between unoccupied and occupied levels in the case of Ni-doped $CoFe_2O_4$ composition [29]. Secondly, the shifting of absorption spectra to lower wavelengths in the case of Ni-doping needed much energy to move an electron from the valence band to the conduction band so more light is absorbed, and the energy band gap value is increased [30].

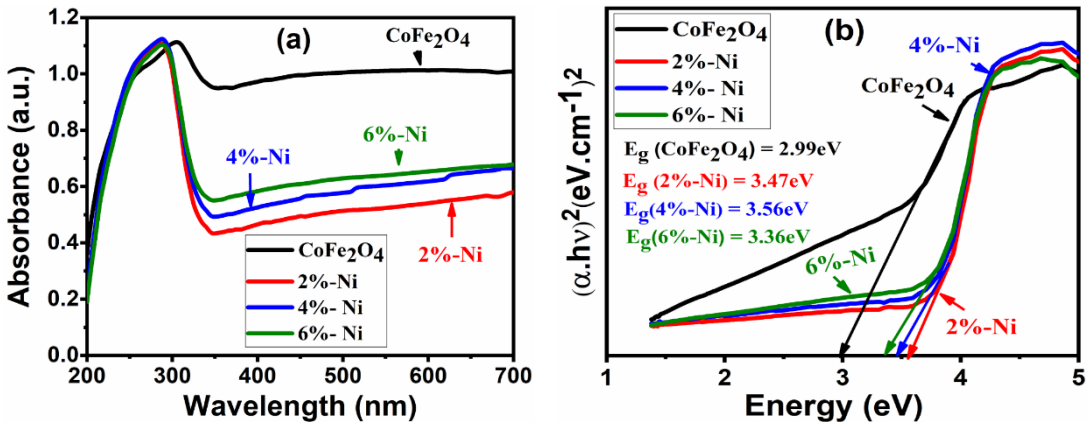

Fig. 5. UV-VIS spectrophotometry results here (a) Absorption spectra, (b) Energy band gap values extracted through Tauc-plot.

3.4. Antibacterial Activities

The antibacterial effect of undoped and Ni-doped $CoFe_2O_4$ compositions was studied against three clinically isolated Staph aureus *(Gram-positive)*, Pseudomonas aeruginosa, and E. Coli *(Gram negative)* bacteria via well-established agar well-disc diffusion route. The variation in concentration (25, 50, 75 and 100 mg/mL) of nanoparticles were tested and their zone of inhibition *(MIC)* measurements with the details of their average values are shown in Figure 6 and in table 3, respectively. The inhibition zone values show enhancement with Ni^{2+} concentration from 3-25 mm as reported in previous work of A. Lagashetty [31]. It can be seen from the figure that the antibacterial sensitivity of these materials shows a high effect against Staph aureus as compared to Pseudomonas aeruginosa and E. Coli. By increasing concentration from 25- 100 mg/mL also enhanced the anti-effect of pure and $CoFe_2O_4$ nanoparticles against these bacteria as reported in kinza et al. work [15]. Advanced oxidation is the very best destruction process used for the conversions of toxic pollutants into nontoxic substances [32]. The theory state that "most of metals oxide have positive ions/charges, while the microorganism possesses negative ions/charges when reactions between them occurred, as a result, electromagnetic attraction phenomena produced as well as oxidation processes happened and finally, death of microorganism occurred". In the current study, distortion and death of bacteria occurred due to a reaction between Ni/Co positive ions and negative ions of microorganisms. Furthermore, the highest Ni-content sample shows a high value of zone of inhibition of 7-22 mm against S. aureus. Similarly, pure $CoFe_2O_4$ also has good results against Gram-positive S. aureus with a high ZOI of 25 mm. Overall, P. Aeruginosa has a lower antibacterial effect as compared to two other bacterial strains due to the reason that Gram-positive have a thinner cell wall as compared to Gram-negative so, its death easily occurred. It can be concluded from the high antibacterial resistance of pure and Ni-doped $CoFe_2O_4$ that these materials can be highly recommended as good candidates for different biomedical applications.

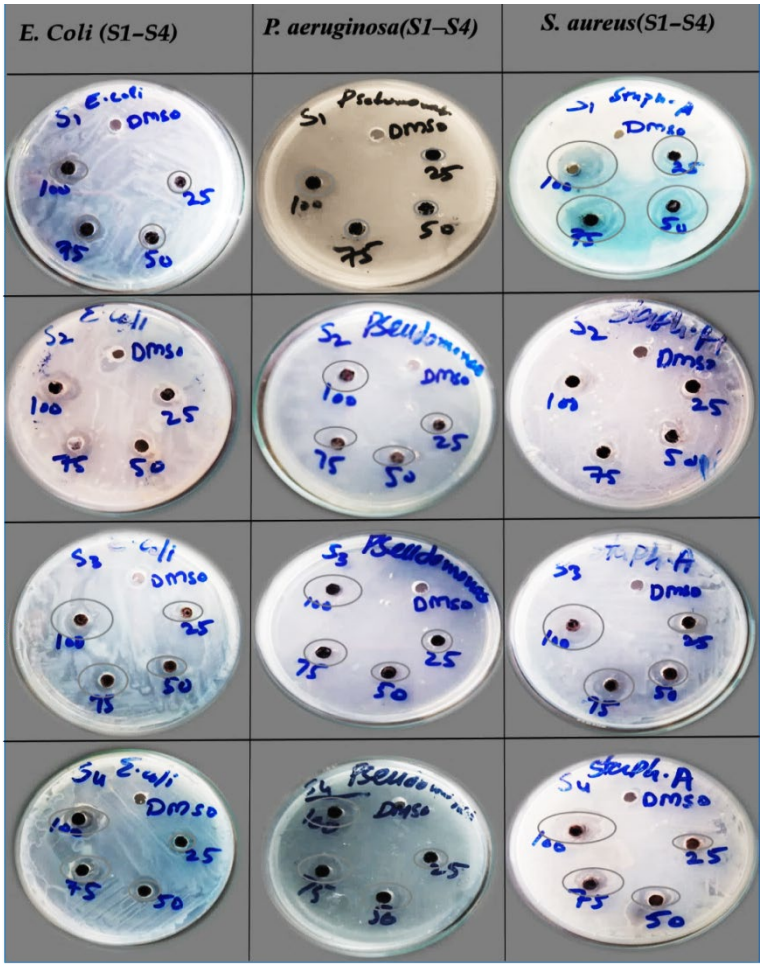

Fig. 6. Anti-bacterial effects images of agar well disc against different bacteria, and here (S1) shows pure $CoFe_2O_4$, (S2) 2 wt.% Ni doped(S3) 4 wt.% Ni doped and (S4) 6 wt.% Ni doped $CoFe_2O_4$ compositions.

Table 3. Zone of inhibition of anti-bacterial effect of pure and Ni doped cobalt ferrite compositions against different bacterial strain.

Samples	*Concentration Mg/mL*	*Zone of Inhibition (mm)*		
		S. aureus (Gram +ive)	*P. aeruginosa (Gram -ive)*	*E. Coli (Gram -ive)*
Pure-$CoFe_2O_4$	25	14	4	3
	50	17	6	7
	70	21	7	10
	100	25	10	12
2% -Ni Doped	25	8	7	5
	50	11	9	8
	70	16	11	11
	100	20	12	14
4% -Ni Doped	25	7	5	6
	50	12	8	10
	70	17	12	15
	100	22	14	18
6% -Ni Doped	25	8	6	4
	50	10	10	9
	70	14	11	12
	100	20	13	16

4. Conclusion

The pure and Ni incorporated $CoFe_2O_4$ nanoparticles were very successfully synthesized via a well-established hydrothermal technique. The x-rays diffraction analysis confirmed crystallinity, and spinel cubic structure with 10.83 nm, 12.21 nm, 14.90 nm, and 17.96 nm crystals size for pure and 2%, 4%, and 6% Ni-doped cobalt ferrite, respectively were recorded. The FESEM and EDX analysis revealed the uniform and spherical shape growth of nanoparticles as well as the presence of Ni, Co, Fe, and O elements present in these compositions. The UV--visible absorption investigation showed that the energy band decreases from 2.98 eV to 2.60 eV with a shift in absorbance to a lower wavelength of electromagnetic radiation. The antibacterial studies demonstrated that the incorporation of Ni-positive ions in $CoFe_2O_4$ compositions enhanced the antibacterial effect against Gram-positive and negative bacteria, and MIC values are observed in the range of 3-25 mm for pure and highest Ni content $CoFe_2O_4$ nanoparticles samples. Finally, it is concluded from optical and antibacterial studies that these materials are highly recommended for photovoltaic and biomedical applications in form of electronic devices and antibiotics, respectively.

Acknowledgments

The authors would like to acknowledge the Researcher's Supporting Project Number (RSP2023R71), King Saud University, Riyadh, Saudi Arabia for their support in this work.

References

[1] K. Pubby, S.S. Meena, S.M. Yusuf, S. Bindra Narang, Journal of Magnetism and Magnetic Materials. 466 (2018) 430-445; https://doi.org/10.1016/j.jmmm.2018.07.038

[2] C. Liu, B. Zou, A.J. Rondinone, Z.J. Zhang, J. Am. Chem. Soc. 122 (2000) 6263-6267; https://doi.org/10.1021/ja000784g

[3] M. Rajendran, R.C. Pullar, A.K. Bhattacharya, D. Das, S.N. Chintalapudi, C.K. Majumdar, Journal of Magnetism and Magnetic Materials. 232 (2001) 71-83; https://doi.org/10.1016/S0304-8853(01)00151-2

[4] K.E. Mooney, J.A. Nelson, M.J. Wagner, Chem. Mater. 16 (2004) 3155-3161; https://doi.org/10.1021/cm040012+

[5] D.H. Lee, H.S. Kim, J.Y. Lee, C.H. Yo, K.H. Kim, Solid State Communications. 96 (1995) 445-449; https://doi.org/10.1016/0038-1098(95)00491-2

[6] M. Grigorova, H.J. Blythe, V. Blaskov, V. Rusanov, V. Petkov, V. Masheva, D. Nihtianova, Ll.M. Martinez, J.S. Muñoz, M. Mikhov, Journal of Magnetism and Magnetic Materials. 183 (1998) 163-172; https://doi.org/10.1016/S0304-8853(97)01031-7

[7] A. Franco Júnior, V. Zapf, P. Egan, Journal of Applied Physics. 101 (2007) 09M506; https://doi.org/10.1063/1.2711063

[8] S.R. Ahmed, P. Kofinas, MRS Proc. 661 (2000) KK10.10; https://doi.org/10.1557/PROC-661-KK10.10

[9] S. Agrawal, A. Parveen, A. Azam, Journal of Magnetism and Magnetic Materials. 414 (2016) 144-152; https://doi.org/10.1016/j.jmmm.2016.04.059

[10] E. Casbeer, V.K. Sharma, X.-Z. Li, Separation and Purification Technology. 87 (2012) 1-14; https://doi.org/10.1016/j.seppur.2011.11.034

[11] S.D. Bhame, A. Bhapkar, M.M. Shirolkar, P.A. Joy, Journal of the Indian Chemical Society. 99 (2022) 100599; https://doi.org/10.1016/j.jics.2022.100599

[12] U. Häfeli, W. Schütt, M. Zborowski, American Institute of Physics, eds., 8th International Conference on the Scientific and Clinical Applications of Magnetic Carriers: Rostock, Germany, 25-29 May 2010, American Institute of Physics, Melville, N.Y, 2010.

[13] V.G. Harris, A. Geiler, Y. Chen, S.D. Yoon, M. Wu, A. Yang, Z. Chen, P. He, P.V. Parimi,

X. Zuo, C.E. Patton, M. Abe, O. Acher, C. Vittoria, Journal of Magnetism and Magnetic Materials. 321 (2009) 2035-2047; https://doi.org/10.1016/j.jmmm.2009.01.004
[14] R. Valenzuela, Physics Research International. 2012 (2012) 1-9; https://doi.org/10.1155/2012/591839
[15] K. Sakhawat, F. Ullah, I. Ahmed, T. Iqbal, F. Maqbool, M. Khan, H. Tabassum, M. Abrar, Appl Nanosci. 11 (2021) 2801-2809; https://doi.org/10.1007/s13204-021-02149-z
[16] M. Atif, M. Nadeem, R. Grössinger, R.S. Turtelli, Journal of Alloys and Compounds. 509 (2011) 5720-5724; https://doi.org/10.1016/j.jallcom.2011.02.163
[17] J. Zhang, J. Shi, M. Gong, Journal of Solid State Chemistry. 182 (2009) 2135-2140; https://doi.org/10.1016/j.jssc.2009.05.032
[18] M.H. Yousefi, S. Manouchehri, A. Arab, M. Mozaffari, Gh.R. Amiri, J. Amighian, Materials Research Bulletin. 45 (2010) 1792-1795; https://doi.org/10.1016/j.materresbull.2010.09.018
[19] Y. Xie, Y. Qian, W. Wang, S. Zhang, Y. Zhang, Science. 272 (1996) 1926-1927; https://doi.org/10.1126/science.272.5270.1926
[20] S. Phumying, S. Labuayai, E. Swatsitang, V. Amornkitbamrung, Santi Maensiri, Materials Research Bulliten. 48 (2013) 2060-2065; https://doi.org/10.1016/j.materresbull.2013.02.042
[21] Y. Cheng, Y. Zheng, Y. Wang, F. Bao, Y. Qin, Journal of Solid State Chemistry. 178 (2005) 2394-2397; https://doi.org/10.1016/j.jssc.2005.05.006
[22] G. Demazeau, J. Mater. Chem. 9 (1999) 15-18; https://doi.org/10.1039/a805536j
[23] K. Sue, K. Kimura, K. Arai, Materials Letters. 58 (2004) 3229-3231; https://doi.org/10.1016/j.matlet.2004.06.016
[24] N. Ullah, M.T. Qureshi, A.M. Toufiq, F. Ullah, M. Al Elaimi, R.S.A. Hameed, A. Khan, H.M.E. Ragab, Appl. Phys. A. 127 (2021) 779; https://doi.org/10.1007/s00339-021-04926-7
[25] J. Ahmad, M. Ehsan Mazhar, M. Qadeer Awan, M. Naeem Ashiq, Physica B: Condensed Matter. 406 (2011) 3484-3488; https://doi.org/10.1016/j.physb.2011.06.031
[26] A. Tirsoaga, D. Visinescu, B. Jurca, A. Ianculescu, O. Carp, J Nanopart Res. 13 (2011) 6397-6408; https://doi.org/10.1007/s11051-011-0392-1
[27] M.M. Naik, H.S.B. Naik, N. Kottam, M. Vinuth, G. Nagaraju, M.C. Prabhakara, J Sol-Gel Sci Technol. 91 (2019) 578-595; https://doi.org/10.1007/s10971-019-05048-6
[28] C.A. Schneider, W.S. Rasband, K.W. Eliceiri, Nat Methods. 9 (2012) 671-675; https://doi.org/10.1038/nmeth.2089
[29] S. Anjum, R. Tufail, K. Rashid, R. Zia, S. Riaz, Journal of Magnetism and Magnetic Materials. 432 (2017) 198-207; https://doi.org/10.1016/j.jmmm.2017.02.006
[30] S. Joshi, M. Kumar, Ceramics International. 42 (2016) 18154-18165; https://doi.org/10.1016/j.ceramint.2016.08.130
[31] S. Demirci, T. Dikici, M. Yurddaskal, S. Gultekin, M. Toparli, E. Celik, Applied Surface Science. 390 (2016) 591-601; https://doi.org/10.1016/j.apsusc.2016.08.145
[32] J. Su, H. Gong, J. Lai, A. Main, S. Lu, Infect Immun. 77 (2009) 667-675; https://doi.org/10.1128/IAI.01027-08